Phase-field investigation of microstructure evolution under the influence of convection

Ricardo da Silva Siquieri, Heike Emmerich

Phase-field investigation of microstructure evolution under the influence of convection

Journal:	*Philosophical Magazine & Philosophical Magazine Letters*
Manuscript ID:	TPHM-10-Jan-0012.R1
Journal Selection:	Philosophical Magazine
Date Submitted by the Author:	08-Apr-2010
Complete List of Authors:	Siquieri, Ricardo; RWTH Aachen University, Computational Materials Engineering, Institute of Minerals Engineering Emmerich, Heike; RWTH Aachen University, Computational Materials Engineering, Institute of Minerals Engineering
Keywords:	crystal growth, numerical simulation, phase transformations
Keywords (user supplied):	dendritic growth, eutectic growth, Peritectic growth
Note: The following files were submitted by the author for peer review, but cannot be converted to PDF. You must view these files (e.g. movies) online.	
figs.tar.gz siquieriPHM.tex.gz	

Philosophical Magazine,
Vol. 00, No. 00, DD Month 200x, 1–23

Phase-field investigation of microstructure evolution under the influence of convection

Ricardo Siquieri and Heike Emmerich,
Computational Materials Engineering, Center of Computational Engineering Science and Institute of Minerals Engineering, RWTH Aachen, Mauerstrasse 5, D-52064 Aachen, Germany

(Received 00 Month 200x; in final form 00 Month 200x)

Numerical simulation of solidification and crystal growth has attracted industrial attention as a powerful engineering tool for processes and alloy optimization. In this work we present a detailed study of the influence of flow on the microstructure evolution during solidification. First, we include convection effects into an existing quantitative phase-field model [Phys. Rev. E, 70 (2004) 061604] that is meant to simulate dendritic growth of a binary alloy. We apply it to investigate the solidification of a Fe-Mn alloy under external flows conditions. In addition, we present an extension of the quantitative phase-field model of two-phase growth [Phys. Rev. E, (2005) 72 011602] that includes natural and forced convection effects in the melt phase. We use this extension to investigate directional solidification of eutectic lamellae under the influence of convection as well as microstructure formation of peritectic growth in the presence of convection.

1 Introduction

The investigation of pattern formation in alloy solidification has been the topic of several research studies, see e.g. [1,2]. The formation of microstructures during solidification plays an important role in determining the properties of nearly all man-made metal products. The simulation of solidification and crystal growth processes has been of growing interest because of its importance in many technological applications. Most theoretical/numerical models on microstructure evolution are based only on diffusive mass transport. The practical relevance of those for real life applications has been questioned by the fact that conditions are only rarely met which permit a direct quantitative comparison with such as theoretical description. Indeed, the description refers to a situation without convection, despite the fact that crystal growth processes almost never occurs in conditions free of convection. Neglecting convection effects is generally motivated by the difficulty of including them in the theory and the argument that the basic prototypes of solidification patterns appear and may be studied without convection. Research under microgravity conditions in the last decades has shown the importance of convection. It has become clear that, even in the best experimental setups used on earth, residual flows can change the microstructure and thus complicate a detailed quantitative comparison with theoretical predictions which do not take convection into account. The systematic analysis of convective effects and its inclusion in theoretical models is complicated as there are many causes for fluid flow. Melt flow in solidification can be categorized into natural and forced convection. Included as natural convection is convection caused by contraction (or expansion) when the densities of the solid and liquid are different regardless of the presence of the gravitational force. Forced convection is due to externally applied conditions, for instance electromagnetic stirring, rotation, pouring of melt, etc., some of which may be intentionally introduced to cause convection to enhance solute transport from the solid-liquid interface in order to reduce macro- and microsegregation. Natural convection is believed to be responsible for the discrepancies between experimental data under terrestrial conditions and the prediction of diffusion-based theories that ignore convection.

Numerical modeling of crystal growth in the solidification of pure metals and alloys remains a significant challenge in material science and applied physics. Even for the most common growth morphology (i.e. dendritic growth) which has been studied over the past two decades, a full numerical simulation for non-dilute metallic alloys with properties found in real castings still remains challenging even in the absence of convection. The difficulties lie in the widely different length and time scales in the coupled energy and mass transport processes, in the segregation of the solute upon solidification and in the strong dependence

Philosophical Magazine
ISSN 1478-6435 print/ISSN 1478-6443 online
http://www.tandf.co.uk/journals
DOI: 10.1080/1478643YYxxxxxxxx

of the melting temperature on the liquidus concentration. When convection is included, the problem is further complicated by the coupling of the Navier-Stokes equations in the presence of evolving solid-liquid interfaces. Melt convection adds new length and time scales to the problem and results in morphologies that are potentially very different from those generated purely by diffusive heat and solute transport.

With the advent of new numerical techniques such problems can be solved with a relatively high order of accuracy and thus it is possible to make predictions which, together with experimental observations, are able to contribute to the understanding of many complicated physical aspects of crystal growth or pattern formation in nature.

The various techniques for the numerical simulation of crystal growth can in principle be divided into two basic groups: explicit interface tracking and the diffuse interface approach. The explicit interface tracking method includes the classical sharp interface approach. The phase-field method together with its variants constitute the diffuse-interface approach.

In this work we use phase-field models and combine them with a numerical approach for the Navier-Stokes equations to investigate the influence of convection on microstructure evolution during solidification.

We concentrate our investigations on the most frequent types of morphology evolution found during cast processes in metal alloys - namely dendritic growth, eutectic lamellae growth and peritectic growth.

The main goal here is to gain new insight into the numerical simulation of crystal growth under the influence of a convection field.

The work is divided in three sections: In the first section we present a quantitative phase-field approach for binary alloy systems and extend it to take into account the influence of fluid flow in the melt phase. The validation of the model is presented and we use it to investigate the influence of convection on dendritic growth for the system Fe-Mn. In the second section, we use the knowledge of the previous section to add the effect of convection to the quantitative phase-field approach by Folch and Plapp. This method is meant to solve eutectic/peritectic growth of binary alloy systems. First, we present the convergence of the model and show that even by coupling the binary phase-field equation with the Navier-Stokes equations we still reproduce quantitative results. Secondly, we present numerical simulations of direction solidification for eutectic growth under the effect of convection and then we show how convection interacts with heterogeneous nucleation and microstructure formation of peritectic alloy systems. Finally we present a summary.

2 Dendritic growth under the influence of convection

In the past 15 years the phase-field method has become the method of choice for simulating microstructure evolution in materials [3, 4]. The methodology is based on approaches from irreversible thermodynamics [4, 5], which have their origin in theoretical descriptions for second-order phase transitions second-order phase transitions.

Phase-field models have the advantage of being proned to generalizations e.g. including the effects of convection in the liquid phase on microstructure development [18], including the contributions of elastic energy to the free energy of the system, and taking into account, in a proper way e.g. the effects of attachment kinetics on the interface on the pattern formation during solidification. Over the past two decades, they have become a standard tool for solving many physical and material science problems. The phase-field approach belongs to a group of methods that rely on treating a microscopically sharp interface as a diffuse region immersed in the calculation domain.

The advantage of the phase-field method is that its evolutionary equations are derived in a thermodynamically consistent manner and there is no need to track the interface, since the interface is part of the solution. The phase-field equations are defined over the whole domain where we introduce the phase-field variable ϕ that varies smoothly e.g. from -1 to 1 between bulk phases over the diffuse interface region of width W (see Fig. 1). The phase field variable ϕ serves to distribute the interfacial forces and other source terms over the diffuse interface region.

The phase field evolution equations are considered to be a relaxation in direction to the minimum of the free energy functional, similar to the time-dependent Ginzburg-Landau models for the out-of-equilibrium thermodynamics of phase transitions [7]. The price to pay for this simple choice of the equations is the

introduction of an interface width W as a new scale into the problem. The typical size of the solid-liquid interface is of the order of nanometers whereas typical microstructural patterns are in the microscale. Hence, the numerically solve of such a multiscale problem is clearly unfeasible. In order to reduce the gap between the scales of the interface thickness and the pattern, the solid-liquid interface needs to be chosen several orders of magnitude thicker than in the real physical problem. Doing so, it is clear that the simulations will become dependent of the choice of W. To overcome this problem Karma & Rappel [1,6] developed the so called *thin-interface limit* of the phase-field model, in which W is considered small but finite and compared to the scale of the pattern, but not smaller than the microscopic capillary length d_0. It was shown that in a thin interface limit the phase-field model reduces asymptotically to the free boundary problem similar to the formal asymptotic limit of vanishing interface thickness but with a modified expression for the kinetic coefficient. The benefits of this limit are a much less restriction on W/d_0 which makes it possible to perform efficient computations and gives the possibility to eliminate interface kinetic effects. But it still produces unphysical effects associated with the thickness of the interface caused by unequal thermalconductivities or unequal diffusivities in solid and liquid phases. To eliminate these effects an anti-trapping term in the diffusion equation for the pure substance was been developed [8], which was recently extended to simulate the solidification of dilute binary alloys [9–11].

While the basic mechanisms of dendritic growth could be understood in many aspects using quantitative phase-field models [1, 10–12], the relevance of this understanding for practical applications has been questioned by the fact that we can have direct quantitative comparisons between the experiments and the theory only in rare conditions.

Generally, this description refers to a situation at a small undercooling and without convection. Because in most real-life situations convection is inevitable, a better understanding of dendritic growth in the presence of flow in the melt is an important theoretical and practical problem.

Under normal growth conditions, i.e. if we do not have a microgravity setup, the inhomogeneous temperature distribution in the solidification sample will produce thermal convection [2, 13]. Even under microgravity the density difference between the two phases induces convection [2, 14, 29]. It is also clear that under gravity, natural convection can substantially influence the growth process and the features of the resulting pattern [2, 13, 15–17].

Numerical simulations of dendritic growth under convection influence for a pure substance have been performed in diverse geometries [13, 17–19] and both with imposed flows and natural convection [2, 13, 15, 17, 20, 21]. For binary alloys much less has been done [2, 13] and many aspects of such processes still have to be investigated. Therefore, we present a phase-field model to investigate the influence of convection on dendritic growth of binary alloys.

Including fluid flow in phase-field models for binary alloys is a very demanding task, basically because fluid flow brings an additional length scale to the model which must be controlled during the simulations.

2.1 *Description of the model*

The approach presented in this work is based on the quantitative phase-field model for binary alloys defined in [10,11]. In our extension, the phase field equations remain unchanged and we assume that the phase-field is not affected by the flow field. A no-slip condition at the solid-liquid interface is enforced by adding a source term [18] in the Navier-Stokes equations. Doing so, the no-slip condition is accurately reproduced regardless of the diffuse interface thickness [18, 19].

We denote ϕ as the phase-field variable, where ϕ varies smoothly from 1 in the solid to -1 in the liquid. The interface is represented by the contour $\phi = 0$, see Fig. 1.

The starting point for developing the model is the free energy functional of the system [10]

$$F = \int_V f(\nabla\phi, \phi, c, T)dV, \tag{1}$$

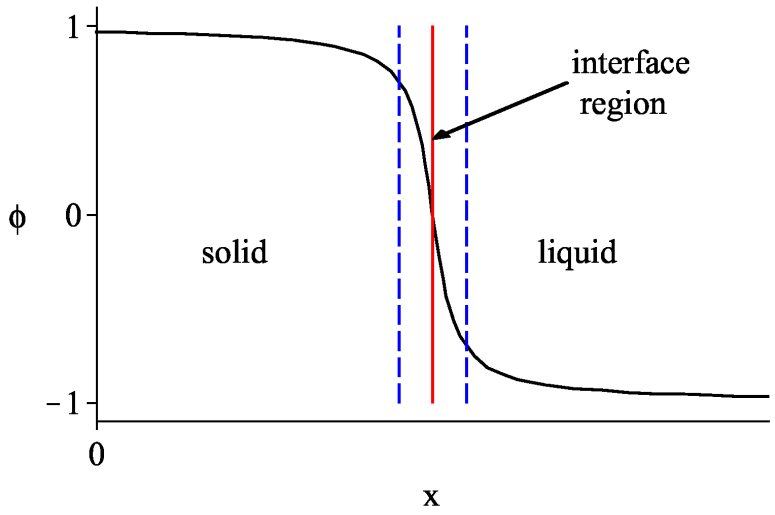

Figure 1. Phase-field profile.

with the free-energy density defined as

$$f(\nabla\phi, \phi, c, T) = K f_{grad}(\nabla\phi) + H f_{\phi}(\phi) + f_c(\phi, c, T), \tag{2}$$

where f_ϕ depends only on the phase-field and provides the double well potential, f_c couples the phase fields to the concentration and temperature; f_{grad} sets a free energy cost for gradients in ϕ, forcing the interface to have a finite width; H is a constant with the dimensions of energy per unit volume and K has the dimension of energy per unit length.

In the variational form the phase field equations read

$$\tau(\phi)\frac{\partial\phi}{\partial t} = -\frac{1}{H}\frac{\delta\mathcal{F}}{\delta\phi} \tag{3}$$

where H is introduced to remove the dimension of $\mathcal{F}$.

The conserved concentration field obeys the continuity equation

$$\frac{\partial c}{\partial t} + (1-\psi)(\mathbf{v}\cdot\vec{\nabla})c + \vec{\nabla}\cdot\vec{J} = 0 \tag{4}$$

where $\mathbf{v}$ is the fluid velocity, ψ is the solid fraction coupled with the phase-field ϕ by $\psi = (1+\phi)/2$, $\psi \in [0,1]$ and $\vec{J}$ is the flux of the scaled concentration c

$$\vec{J} = -M(\phi, c)\vec{\nabla}\frac{\delta\mathcal{F}}{\delta c} \tag{5}$$

with $M(\phi, c)$ being a mobility.

Taking the appropriate form for f_{grad}, f_ϕ, f_c and switching to a non-variational formulation, for reasons described in reference [10], we can write the phase-field equation as

$$\begin{aligned}\tau(\theta)\frac{\partial\phi}{\partial t} = \vec{\nabla}\cdot[W(\theta)^2\vec{\nabla}\phi] + \partial_x\left(|\vec{\nabla}\phi|^2 W(\theta)\frac{\partial W(\theta)}{\partial(\partial_x\phi)}\right) \\ +\partial_y\left(|\vec{\nabla}\phi|^2 W(\theta)\frac{\partial W(\theta)}{\partial(\partial_y\phi)}\right) + \phi - \phi^3 - \tilde{\lambda}(1-\phi^2)^2\left(c_l - c_l^0\right).\end{aligned} \tag{6}$$

Note that we include anisotropy in the model by making W and τ orientation dependent [1]

$$W(\theta) = W a_s(\theta) = W(1 + \epsilon_4 \cos(4\theta)), \tag{7}$$

$$\tau(\theta) = \tau a_s(\theta)^2, \tag{8}$$

where $W = \sqrt{K/H}$, $\theta = \arctan(\partial_y\phi/\partial_x\phi)$, is the angle between the direction normal to the phase-field interface and the x axis, and ϵ_4 is the anisotropy strength.

The modified coupled constant $\tilde{\lambda}$, which is associated with the driving force of the solidification, is defined by using $W = \gamma/IH$, as it was described by Echebarria et al. [10]

$$\tilde{\lambda} = \frac{a_1 LW}{\gamma} = \frac{L}{JH} \tag{9}$$

with $a_1 = I/J$, $I = 2\sqrt{2}/3$ and $J = 16/15$.

In our simulations we set the kinetic effect to zero according to an analysis of the thin-interface limit derived by Karma et al. [1,6]:

$$\tau = \frac{a_2 \lambda W^2}{D} \tag{10}$$

with $a_2 = 0.6267$, $\lambda = a_1 W/d_0$ and $d_0 = \gamma/Lc_l^0(1-k)$. Note that, this relation is valid for the system with a small convection flow which corresponds to a small Peclet number $Pe = V_\infty R_{tip}/2D \ll 1$. Here V_∞ is a velocity of the flow, R_{tip} is a mean radius of a dendritic tip. In case of large flow velocities the asymptotic analysis of the phase field equations leads to the relation for the kinetic coefficient in the following form

$$\beta = a_1 \frac{\tau(T)}{\lambda W}\left[1 - a_2\lambda \frac{W}{\tau V_\infty}\right],$$

where the flow velocity plays the role of the diffusion.

The diffusion equation eq. (4) is extended by the anti-trapping term and is rewritten in terms of the concentration in the liquid phase as

$$h(\phi)\frac{\partial c_l}{\partial t} = \vec{\nabla}\left(Dq(\phi,k)\vec{\nabla}c_l - a(\phi)W(\theta)c_l(1-k)\frac{\partial\phi}{\partial t}\frac{\vec{\nabla}\phi}{|\vec{\nabla}\phi|}\right)$$
$$-(1-\psi)(\mathbf{v}\cdot\vec{\nabla})c_l + \frac{1}{2}\frac{\partial\phi}{\partial t}c_l(1-k), \tag{11}$$

where $a(\phi)$ according to asymptotic analysis of Echebarria [10] for the giving functions $h(\phi)$ and $q(\phi,k)$ is defined as

$$a(\phi) = \frac{(\phi-1)(1-q(\phi,k))}{\sqrt{2}(\phi^2-1)} = \frac{(kD - D_s)}{2\sqrt{2}kD}. \tag{12}$$

with $k = c_s^0/c_l^0$ being the partition coefficient, which couples the equilibrium concentrations in liquid c_l^0 and solid c_s^0 phases according to the phase diagram.

The presented phase field equations (6) and (11) can be transformed to the equations of Echebarria (eqs. (132-133) in [10]) by replacing of $c_l - c_l^0$ by dimensionless supersaturation $U(\phi)$. There is only the difference in the function $q(\phi)$.

The fluid motion is described by the modified Navier-Stokes equations

$$\frac{\partial(1-\psi)\mathbf{v}}{\partial t} = -(1-\psi)(\mathbf{v}\cdot\vec{\nabla})\mathbf{v} - (1-\psi)\vec{\nabla}\frac{p}{\rho_0} + \vec{\nabla}[\nu\vec{\nabla}(1-\psi)\mathbf{v}] + M_1^d, \tag{13}$$

where p is the pressure, ρ_0 is the liquid density, ν is the the kinematic viscosity and M_1^d is a dissipative interfacial force per unit volume [19] given by

$$M_1^d = -2h\nu\frac{\psi^2(1-\psi)}{W^2}\mathbf{v}, \tag{14}$$

with h being a constant.

The conservation equation for mass takes the following form:

$$\vec{\nabla}\cdot[(1-\psi)\mathbf{v}] = 0. \tag{15}$$

Further in the numerical simulation in Section 2.3 we used the model of Echebarria extended by the convection flow in the form of eqs. (6) - (15) in the dimensionless form as it was carried out in our previous simulations of similar problems [3].

2.2 *Numerical approach*

We use the model equations described in the previous section to numerically simulate dendritic growth of dilute binary alloys under the influence of an imposed flow field. The equations (6)-(15) are numerically discretized using a finite difference approach on an uniform spatial lattice with grid space Δx. We adopt second order discretization for the high order terms and an advanced first order approximation for the terms of low orders. To avoid numerical instability due convective transport, the convective term is discretized by using the up-wind scheme [22]. The phase-field equations are solved using an explicit Euler method with constant time step Δt. To solve the modified Navier-Stokes equations (13) a special scheme is required.

The equations (6)-(15) are discretized employing a finite difference approach, as discussed above. Nevertheless, there is a need to rearrange the components in a staggered grid. To solve the Navier-Stokes equations we use a scheme which is based on the SMAC [23] method. We treat the term (14) implicitly and the convective part of the Navier-Stokes equations explicitly. The resulting system of equations is solved by an iterative Gauss-Seidel method [24]. The system is solved until $\nabla\cdot\widetilde{\mathbf{v}} \approx 0$ and the convergence of the method is controlled (in its explicit part) by

$$\Delta t < \Delta x^2/2D, \tag{16}$$

due to the diffusion field and the convective part through the Courant-Friedrichs-Levy (CFL) condition [22]

$$\Delta t < \Delta x/\widetilde{\mathbf{v}}, \tag{17}$$

where $\widetilde{\mathbf{v}}$ is the dimensionless fluid velocity [3].

In its implicit part the convergence is controlled by limiting the maximum relative error like

$$\mathrm{MAX}\left|\frac{\widetilde{\mathbf{v}}_i^{t+\Delta t} - \widetilde{\mathbf{v}}_{i+1}^{t+\Delta t}}{\widetilde{\mathbf{v}}_i^{t+\Delta t}}\right| < \epsilon_{error}, \tag{18}$$

where ϵ_{error} is a small constant.

The simulation domain is schematically illustrated in Fig. 2. A small crystal seed exists initially in the center of the domain. The seed is engulfed in a supersaturated melt at composition c_l^{in} under forced flow conditions. As shown in figure 2, for symmetry reasons, only half of the domain is simulated. If flow is not considered, then the domain can still be reduced to only a quarter of the total domain of simulation.

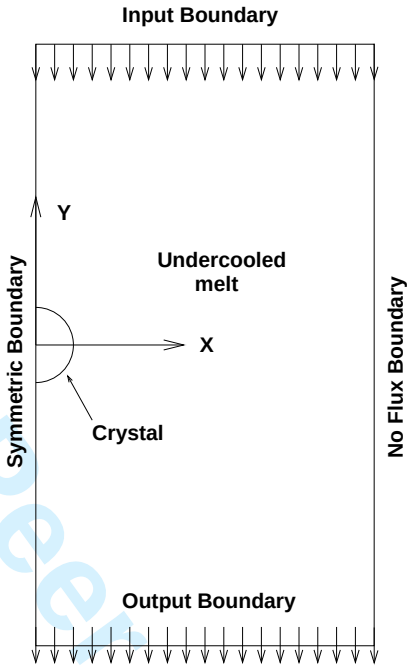

Figure 2. Computational configuration for the dendritic growth simulations.

The crystal axes are aligned with the coordinate axes. For these studies, we apply symmetric boundary conditions on the left side of the domain for all the fields ($\partial v_x/\partial x = 0$, $\partial \phi/\partial x = 0$, $\partial c/\partial x = 0$, $\partial p/\partial x = 0$ and $v_y = 0$). On the right side we use no-flux boundary conditions for the phase field and free-slip boundary condition for the flow field ($\partial v_x/\partial x = 0$, $\partial \phi/\partial x = 0$, $\partial c/\partial x = 0$, $\partial p/\partial x = 0$ and $v_y = 0$). On the top and bottom side we alternated constant inflow ($v_x = 0$, $v_y = V_\infty$, $\partial \phi/\partial y = 0$, $\partial c/\partial y = 0$ and $\partial p/\partial y = 0$) and outflow ($v_x = 0$, $\partial v_y/\partial y = 0$, $\partial \phi/\partial y = 0$, $\partial c/\partial y = 0$ and $\partial p/\partial y = 0$) boundary conditions.

2.3 *Numerical simulations*

In this section we investigate the influence of an imposed flow on the the solidification of a Fe-Mn alloy. All calculations are performed for the isothermal case $T = 1474\,^{\circ}$C and for an initial alloy composition $c_l^{in} = 9.8$ mol% Mn. In Fig. 3 we show the phase-diagram of the Fe-Mn system and a zoom in the region of interest for our simulations. The thermodynamic material parameters of the Fe-Mn alloy (see Ref. [25]) used in the phase-field simulations are: Diffusion coefficient of Mn in liquid $D = 1.0 \times 10^{-9}$ m^2/s, in solid $D_s = 1.0 \times 10^{-12}$ m^2/s, the partition coefficient $k = 0.72$, the anisotropy of the interfacial free energy is taken as $\epsilon_4 = 0.05$.

We used $W = 1.25\Delta x$ and $W/d_0 = 19.25$ in all the simulations. These relations correspond to $\Delta x = 5.9 \times 10^{-7}$m, $d_0 = 3.836 \times 10^{-8}$ m, the solid/liquid interface energy $\gamma = 0.4$ J/m^2 and the latent heat $L = 3.8 \times 10^8$ J/m^3 [26].

During the numerical calculation of the equations (6)-(15) we add a stochastic noise at the interface region in order to include fluctuations at the interface, which gives rise to the initial morphological instability.

In Fig. 4 we show the phase-field simulations of dendritic growth with and without flow. On the left side we present the time evolution of a dendritic growing under purely diffusive conditions. On the right side we present the case where the dendrite grows under forced flow conditions. The total domain size was

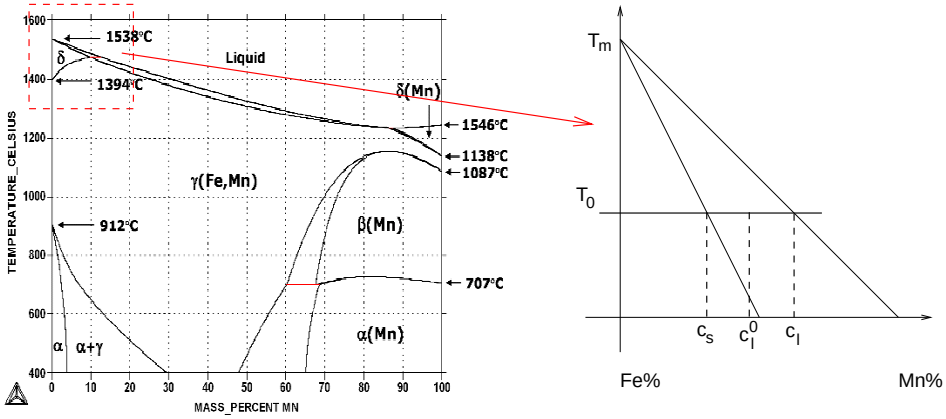

Figure 3. Fe-Mn phase-diagram and a zoom in the region of $c_l^{in} = 9.8$ mol% Mn.

assumed to be $2000W \times 1000W$ in our simplified domain. Note, however that in Fig. 4 as well as in the other snapshots in this section we only show the region near the solid phase (the dendritic one).

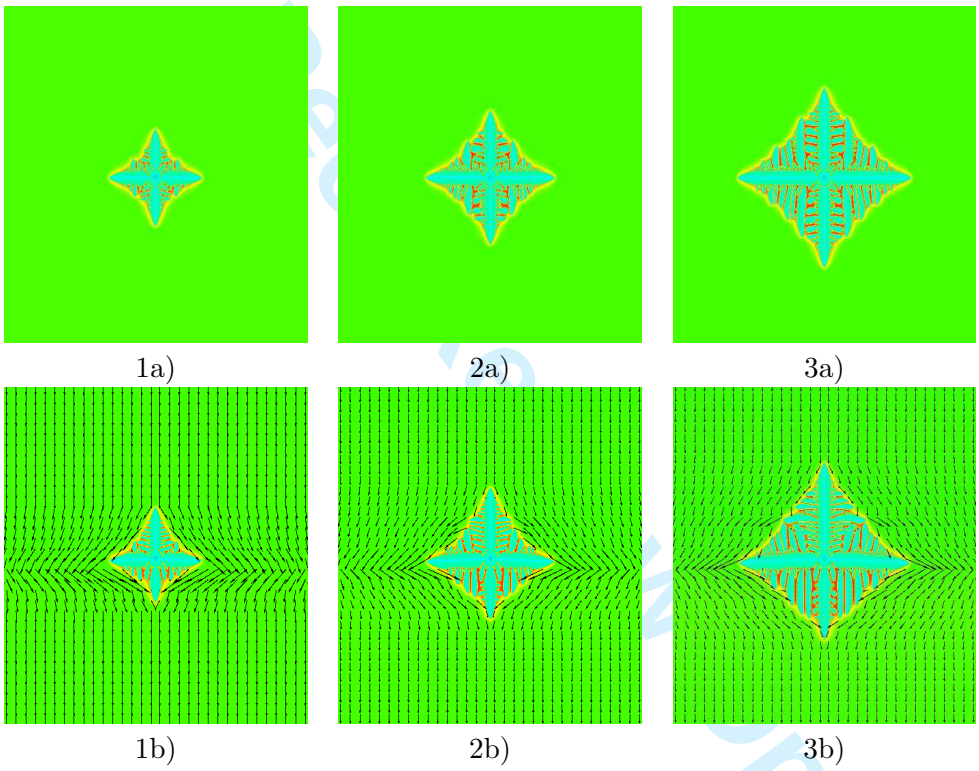

Figure 4. Phase-field simulation of dendritic growth of Fe-9.8 mol% Mn alloy. The time evolves from top to bottom. a) Purely diffusive growth conditions b) With an imposed inflow velocity $V_\infty = 2\mu$m/s.

A further comparison between the simulations show that convection decisively disturbs the symmetry of the equiaxed dendrite. At first, in the case without convection, all the primary dendrites grow with approximately equal velocities from the central nucleus. Secondly, sidebranches emanate from each main arm equally to the right and to the left side, showing approximate mirror symmetry in relation to the axis of the arm (see Fig. 4a)). In the case with convection, one easily notes that the growth velocity of the primary dendrite growing upstream is higher than that of the primary ones growing horizontally, which is, in turn, higher than that of the primary dendrite growing downstream. This can be explained as follows: In the pure diffusive situation, each dendrite has approximately the same growth conditions because the solute boundary layer looks the same for each dendrite, i.e. the height of the solute pile-up is the same

for each dendrite and also the thickness of the boundary layer is the same for each arm in equivalent regions. According to the phase-diagram Fig. 3, an increase in solute content brings about a decrease of the liquidus temperature, which tends to make the growth slower. In the case with convection, the solute boundary layer becomes unsymmetrical. In the region of the upstream growth, the flow steadily supplies fresh liquid (with the nominal alloy composition) to the phase front which keeps the supersaturation high and stimulates the growth. This is confirmed by the fact that, in this case, the pile-up is lower and the thickness of the boundary layer is smaller than in the situation without flow, see Fig. 5. On the other side, in the region of the downstream flow (wake region), there is an excess of solute, which tends to inhibit the growth by decreasing the local supersaturation. This is reflected in a higher solute pile-up and thicker boundary layer in comparison to the situation without flow, see Fig. 5.

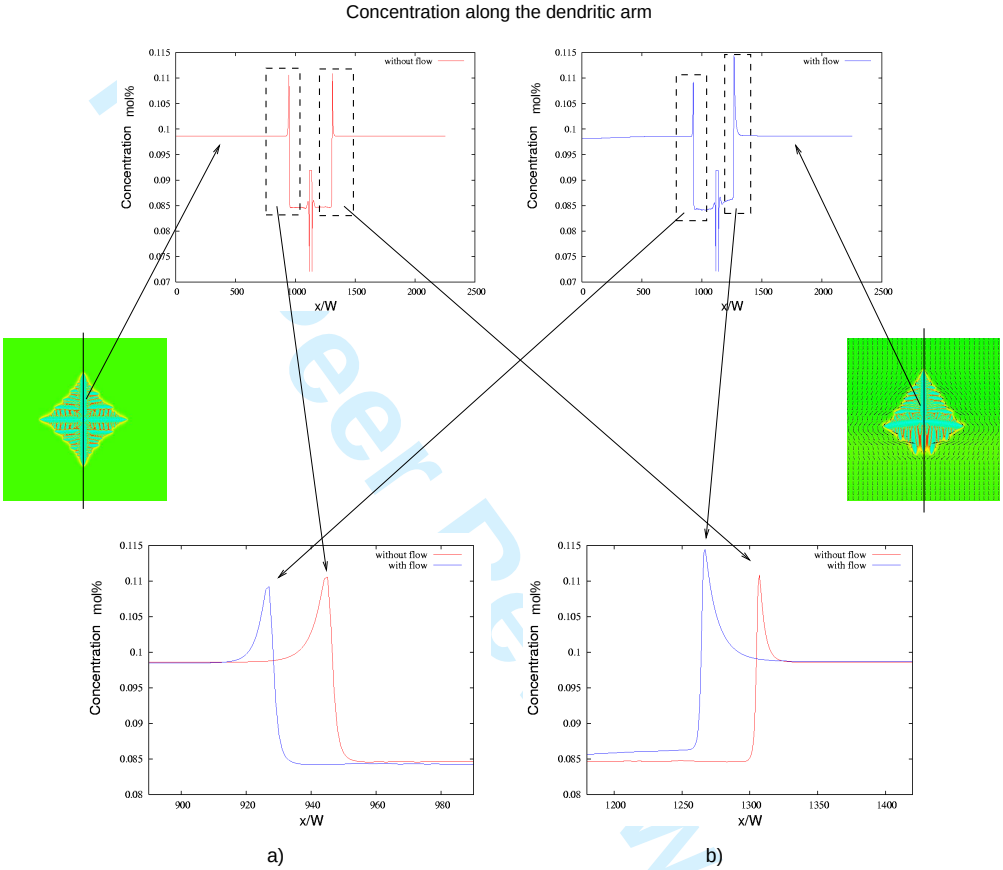

Figure 5. In this picture we compare the solute pile-up in front of the a) the upstream dendritic tip and b) the downstream tip, for the case with and without flow.

As a consequence of the stimulated growth in the upstream direction, the corresponding primary dendrites have the chance of emanating sidebranches earlier than the primary dendrites growing horizontally. The growth of these sidebranches tend to block the growth of the sidebranches from the dendrites growing horizontally. The opposite occurs in the case of the primary dendrite growing downstream. Because its growth is inhibited, its sidebranches lose the competition against the sidebranches of the neighboring horizontal dendrites.

A comparison of the evolution of the dendritic microstructure for different values of the imposed inflow velocity shows that the primary dendrites, which, in the situation without flow, grow along a perfectly horizontal line, deviate from this direction when the inflow velocity is progressively increased. The deviation of the tip from the original horizontal line increases with an increase of the inflow velocity, see Fig. 6. In figure 6 we plot the inflow velocity versus the angle formed between the horizontal line and the tip of the dendrite main stem growing along the horizontal direction (see Fig. 6 on the left side). This asymmetry is brought about by the imposed flow and is related to the changes of local concentration (and consequently,

local supersaturation) which are caused by the flow.

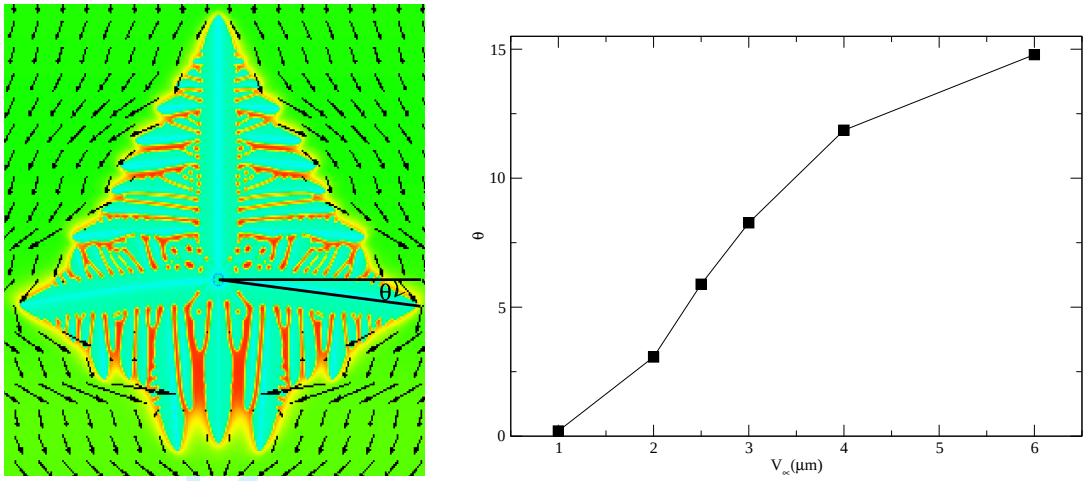

Figure 6. On the left side we show a sketch describing the angle formed between the horizontal line and the tip of the dendrite main stem growing along the horizontal direction. On the right side we show how this angle depends on the inflow velocity.

Observing Fig. 4 and Fig. 6, we note that the envelope of the equiaxed grain for the purely diffusive case corresponds to a square with concave sides (from the outside). This concavity tends to disappear in the upper half of the equiaxed dendrite when the flow is introduced in the system and its velocity is progressively increased. In addition to this, the sidebranches emanating from the upstream growing dendrite seem to "reorient" themselves with an increasing flow velocity, from an orientation which is initially orthogonal to the main arm (as it is usual for diffusive dendritic growth) to another one, which tends to be parallel to the flow lines (mainly for the highest inflow velocities). The number of sidebranches of the upstream growing primary dendrite also tends to reduce with increasing growth velocity, as if convection would stabilize the interface.

3 Quantitative phase-field modelling of two-phase growth with fluid flow

In this section we present an extension of the quantitative phase-field model proposed by Folch & Plapp [9] to investigate the influence of fluid flow on the two-phase solidification of binary alloy systems. The model approach for purely diffusive growth is described in detail in reference [9]. Originally, the phase-field model of Folch & Plapp [9] was developed having its bases on the model approach described in section 2.1. This was one of the first models that allowed for quantitative simulations of low-speed eutectic and peritectic solidification under typical experimental conditions. The extension to incorporate fluid flow in the melt phase allows us to simulate two-phase growth of binary alloys in the presence of convection. In the following section we will give a brief description of the phase-field approach given by Folch and Plapp and explain how we have extended it to incorporate convection in the melting phase. The results in this section will be presented in two parts. First we will present the influence of convection on the growth of eutectic systems and then we will study heterogeneous nucleation and microstructure formation of peritectic growth in the presence of convection.

3.1 *Description of the model*

In the following we extend the phase-field model described in [9] to simulate eutectic/peritectic growth including hydrodynamic convection in the molten phase. We use three phase fields, with $p_i \in [0,1]$ and $p_\alpha + p_\beta + p_L = 1$. p_i label the Alpha phase for $i = \alpha$, Beta phase for $i = \beta$ and liquid phase for $i = L$, respectively. We denote $\vec{p} \equiv (p_\alpha, p_\beta, p_L)$.

The model approach is based on the free energy functional of a representative volume of the investigated material system, which is given by

$$\mathcal{F} = \int_V \sum_i \frac{W(\theta_i)^2}{2}(\nabla p_i)^2 + f dV, \tag{19}$$

where $W(\theta_i) = W(1 + \epsilon_{p_i} \cos 4\theta_i)$ depends on the orientation of the solid-liquid interface [6], with $\theta_i = \arctan \partial_y p_i / \partial_x p_i$ and ϵ_{p_i} being the measure of the anisotropy[1]. The free-energy density is defined as

$$f = \sum_i {p_i}^2(1-p_i)^2 + \widetilde{\lambda}\left[\frac{1}{2}[c - \sum_i A_i(T) g_i(\vec{p})]^2 + \sum_i B_i(T) g_i(\vec{p})\right], \tag{20}$$

where $\widetilde{\lambda}$ is a coupling constant given by

$$\widetilde{\lambda} = \frac{W}{\bar{d}} \frac{a_1}{2}\left(\frac{1}{|A_\alpha|} + \frac{1}{|A_\beta|}\right),$$

with $\bar{d} = (d_\alpha + d_\beta)/2$ being the average capillary length[2] and $a_1 = \sqrt{2}/3$. The function g_i couples the phase-field to the concentration and the temperature. The coefficients $A_i(T)$ and $B_i(T)$ define the equilibrium phase diagram [27] and they can be defined for isothermal solidification or for directional solidification [9]. For the isotherm case they read:

$$A_i(T) = c_i + (k_i - 1)U_i, \quad A_L = 0,$$
$$B_i(T) = A_i U_i \quad B_L = 0,$$

where $U_i = (T_R - T)/(|m_i|\Delta C)$ is the dimensionless undercooling, k_i are the partition coefficients, A_L, B_L are the corresponding liquid coefficients, m_i are the liquidus slope and $c_i = (C_i - C_R)/\Delta C$ is the scaled concentration, where C_R is the liquidus concentration at a certain reference temperature T_R. We use $\Delta C = c_\beta - c_\alpha$. For directional solidification they can be written as:

$$A_i(T) = c_i + (k_i - 1)\frac{z - v_p t}{l_T^i}, \quad A_L = 0,$$
$$B_i(T) = \mp A_i \frac{z - v_p t}{l_T^i} \quad B_L = 0,$$

where v_p is the pulling speed, t is the time and $l_T^i = |m_i|\Delta C/G$ are the thermal lengths, and G is the thermal gradient.

The dynamic of the phases is derived from the free energy functional $\mathcal{F}$ as

$$\tau(\vec{p})\frac{\partial p_i}{\partial t} = -\frac{1}{H}\frac{\delta \mathcal{F}}{\delta p_i}, \tag{21}$$

where $\tau(\vec{p})$ is a relaxation time. In this work we neglect interface kinetics (low undercooling), by choosing $\tau_i = a_2 A_i^2 \widetilde{\lambda} W^2/D$, with $a_2 = 1.175$.

[1] here we consider ϵ_{p_β} always equal to zero

[2] The capillary length for each phase is defined as $d_i = \frac{\sigma_{iL} T_R}{L_i |m_i| \Delta C}$, where L_i are the latent heat of fusion per unit volume, T_R is a reference temperature and σ_{iL} are the solid-liquid surface tensions

The concentration field is given by:

$$\frac{\partial c}{\partial t} + p_L(\mathbf{v}\cdot\vec{\nabla})c - \vec{\nabla}\cdot(M(\vec{p})\vec{\nabla}\frac{\delta\mathcal{F}}{\delta c} - \vec{J}_{AT}) = 0, \tag{22}$$

where $M(\vec{p})$ is a mobility and $\vec{J}_{AT}$ is the anti-trapping term [9] given by

$$\vec{J}_{AT} = 2aW\hat{n}_L\sum_{i=\alpha,\beta}(A_L(T) - A_i(T))(-\hat{n}_L\cdot\hat{n}_i)\frac{\partial p_i}{\partial t}, \tag{23}$$

where $\hat{n}_i = \vec{\nabla}p_i/|\vec{\nabla}p_i|$.

The flow field is modeled by coupling the Navier-Stokes equations to the phase-field [27],

$$\frac{\partial p_L\mathbf{v}}{\partial t} = -p_L(\mathbf{v}\cdot\vec{\nabla})\mathbf{v} - p_L\vec{\nabla}\frac{p}{\rho_0} + \nabla[\nu\nabla p_L\mathbf{v}] + p_L\beta_c\mathbf{g} - 2h\nu\frac{\mathbf{v}}{W^2}p_L^2, \tag{24}$$

$$\vec{\nabla}\cdot p_L\mathbf{v} = 0. \tag{25}$$

where $\beta_c = \frac{\partial\rho}{\partial c}\frac{1}{\rho_0}(c-c_0)$ is the coefficient of solutal expansion, p is the pressure, ν is the kinematic viscosity, ρ_0 is the liquid density and $\mathbf{g}$ is the gravitational constant.

The set of equations (21)-(25) are made dimensionless by using the same scale parameters as discussed in section 2.1, more details about the dimensionless system of equations can be seen in the reference [9].

For the set of equations in this section we use a similar numerical procedure as described in section 2.1. The equations (21)-(25) are discretized using a finite difference approach and we use an Euler explicit scheme to solve the phase-field equations (21)-(22) and a semi-implicit scheme to solve the Navier-Stokes equations (24)-(25).

As part of the optimization/implementation procedure we compute the equation (21) for p_α and p_β only and use the fact that $p_L = 1 - p_\alpha - p_\beta$ to identify the liquid phase.

The model approach described in this section can be used to simulate solidification processes of binary alloys with an Eutectic/Peritectic phase diagram and it also take into account the effect of natural/forced convection in the molten phase. Next, we will use our numerical implementation to investigate typical problems of eutectic/peritectic microstructure evolution under the influence of convection.

Before starting the description of the simulations, it is useful to write down some reference non-dimensional numbers which will be used as parameters in the simulations. When fluid flow is added, we define the flow Peclet number as $P_{ef} = V_\infty H/D_L$, where V_∞ is a reference flow velocity in the system and H is a reference length (to be defined in the individual cases). The solutal Rayleigh number is defined as $Ra = gH^3\beta_c\Delta C/\nu D_L$.

4 Eutectic growth under the influence of convection

An eutectic alloy is characterized by having a composition at which the melting temperature of the alloy is minimal. At this composition, which we call the eutectic composition, the liquid can coexist with two distinct solid phases of different compositions (see Fig. 7).

The formation of lamellar microstructures during eutectic solidification (see Fig. 8) has been intensively investigated, both from the point of view of engineering applications and from the theoretical point of view [28, 29].

Many of these studies are based on the classical theory of Jackson and Hunt [30] for the lamellar and rod-like eutectic growth.

Over the years many authors have discussed the need to take convection effects into account for the simulation of eutectic lamellae growth [28, 31].

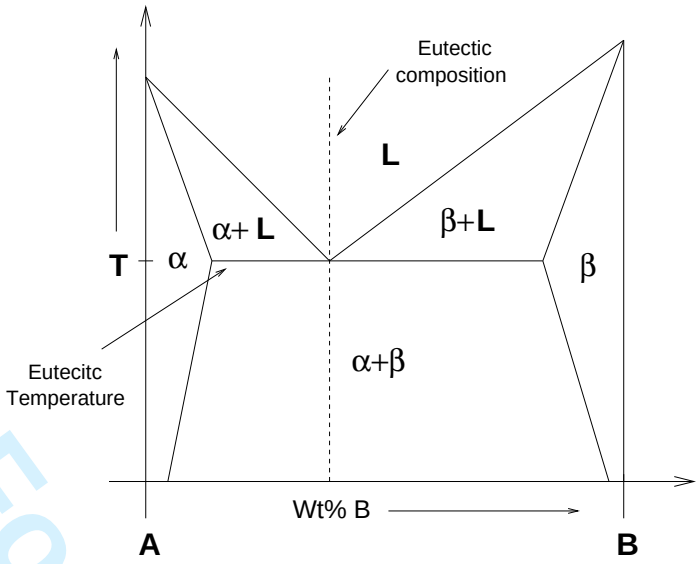

Figure 7. Schematic eutectic phase diagram of an A-B alloy.

It is known that convection can not be avoided in a solidification process and that it drastically alters the dynamic of the growth microstructure. The origin of convection can be natural phenomena - a case we call natural convection - or externally applied phenomena as magnetic stirring, rotation, etc. The influence of convection on eutectic growth has been a field of many controversial studies; the discussion started in 1976 when Larson reported his Apollo-Soyuz Test Project (ASTP) experiment that directional solidification in microgravity causes a significant reduction in the fiber spacing of the MnBi-Bi eutectic [32]. Since Larson's ASTP experiment on MnBi-Bi, a large number of experimental and theoretical studies has been performed to try to understand the influence of convection on eutectic microstructure - see [29, 33] and references therein. Among them, Baskaran and Wilcox [33] have performed numerical calculations on the uniform shear-flow system. Ma *et al.* [31] studied the effect of a weak convection by using analytical perturbation methods taking the flow shear rate as a small parameter. Coriel et al. [14] extended the Jackson-Hunt model to the case where fluid flow is induced by the different densities of the phases. In their studies they showed that the eutectic spacing (see Fig. 8) can increase, decrease, or remain constant in a low-gravity environment, depending on the alloy system. Lee et al. [29] have carried out experimental investigations in Al-Cu systems to study the effect of fluid flow on eutectic microstructures. They showed how different modes of convection can influence the eutectic spacing and the microstructure growth. Zhang et al. [34] carried out numerical studies where they describe changes on the lamellae spacing due to an imposed transverse flow ahead of the solidified interface. They showed that transverse fluid flow increases the interlamellar spacing and that fluid flow strongly alters the microstructure growth.

Although there have been many investigations about eutectic growth under convection effects, none of these studies have considered the phase-field approach. In order to cover this research field in the state of the art on microstructure solidification, we developed a quantitative phase-field model which is able to simulate the growth of lamellae taking into account the effect of natural and forced convection in the melt phase.

4.1 *Numerical simulations*

In this section we perform numerical simulation of directional solidification of eutectic lamellae. In figure 8 we show an example of the two-dimensional lamellae geometry we will simulate.

We apply periodic boundary conditions on the left/right side of the domain, symmetric boundary conditions on the top and no-flux boundary conditions on the bottom. The total simulation box is chosen to be $n_x \times n_z$, where n_x and n_z are the number of grid points perpendicular and parallel to the thermal gradient, respectively. Typically, the number of grid points required in the z direction is much larger than in the x direction, since diffusion and thermal lengths are much larger than the lamellar spacing.

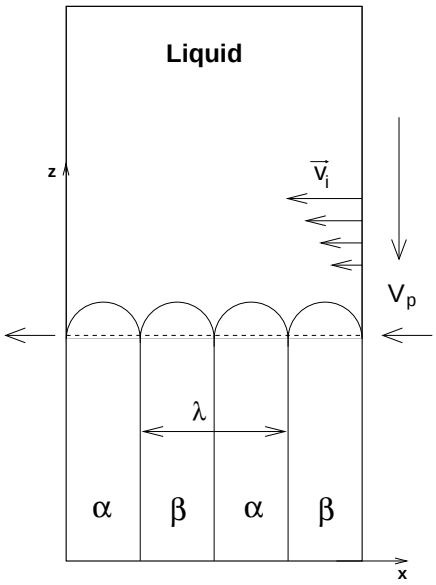

Figure 8. Schematic illustration of eutectic lamellae growth with fluid flow. λ is the lamellar spacing.

Moreover, we start with completely flat interfaces, and the phase fields are initialized as step functions. These step functions then quickly relax to the smooth solutions for the phase fields, while the interfaces begin to curve and drift to adjust their average undercooling. We consider the one-sided model. To allow long time run observation, our numerical scheme is implemented in a frame which follows the solidifying front. This is done by shifting the simulation box from time to time along the growth direction.

Basically we will investigate two types of convection in directional solidification: one is convection caused by a concentration difference in the system, the so called natural convection or buoyancy convection, the second is convection induced by an imposed shear flow ahead of the solidifying front (forced convection).

4.2 *Effect of natural convection on the growth of eutectic lamellae*

Before we start to use the model described in section 3.1, we need first to test its convergence. In reference [9] Folch and Plapp show that the model presented in section 3.1 - for the case where fluid flow is neglected - is convergent to the thin-interface limit. This was done by performing a series of simulations where they fix the physical parameters and decrease the interface width W. They showed that the results become independent of the choice of W for $\lambda/W >= 64$ (in their parameters range). Their results were compared with the numerical solution obtained from the boundary integral model.

In this section we test the convergence of our approach by investigating the steady state lamellar growth when natural convection is taken into account in the liquid phase. We perform the same series of simulations as described in Ref. [9]. Unfortunately, we can not compare our results with a sharp-interface approach since to our knowledge there is no sharp-interface approach for eutectic problem with fluid flow.

We adopt the same input parameters as given in [9]: we take $l_D/\bar{d} = 51200$ and $\bar{l}_T/l_D = 4$ where $l_D \approx D/v_p$ is the diffusion length. This corresponds to the typical experimental values $G \approx 100K/cm$ and $v_p \approx 1\mu m/s$ for CBr_4-C_2Cl_6 [35]. We use $m_\alpha = -m_\beta$, $c_\alpha = -c_\beta$ (symmetric phase diagram) and eutectic composition in the liquid. For the fluid flow we take $Ra = 1.34 \times 10^{-2}$ and $Ra = 3.85 \times 10^{-2}$. We compute the solutal Rayleigh number based on the thickness of the solutal boundary layer where the concentration gradient exists. We define this thickness as the distance from the interface to the position where the concentration drooped 99% in the boundary layer. Following the simulations given in reference [9] the tests are done by decreasing W (increasing λ/W) while keeping all the ratios above and λ/λ_{min} fixed, where $\lambda_{min} \propto \sqrt{\bar{d}l_D}$ is the minimum undercooling spacing. Thus, we take $\lambda/W = 32$, 64, 96 and 128, and fix all others ratios. For each simulation, the interface profile and the interface undercooling are monitored to check when the steady state is reached. As you can take from figure 9 the convergence in the case with convection is somewhat slower than in the case without convection. Note that the results for $\lambda/W = 32$

are not plotted in figure 9, since they are far from the converged lamellae profile. Nevertheless, we achieve convergence for $\lambda/W >= 96$.

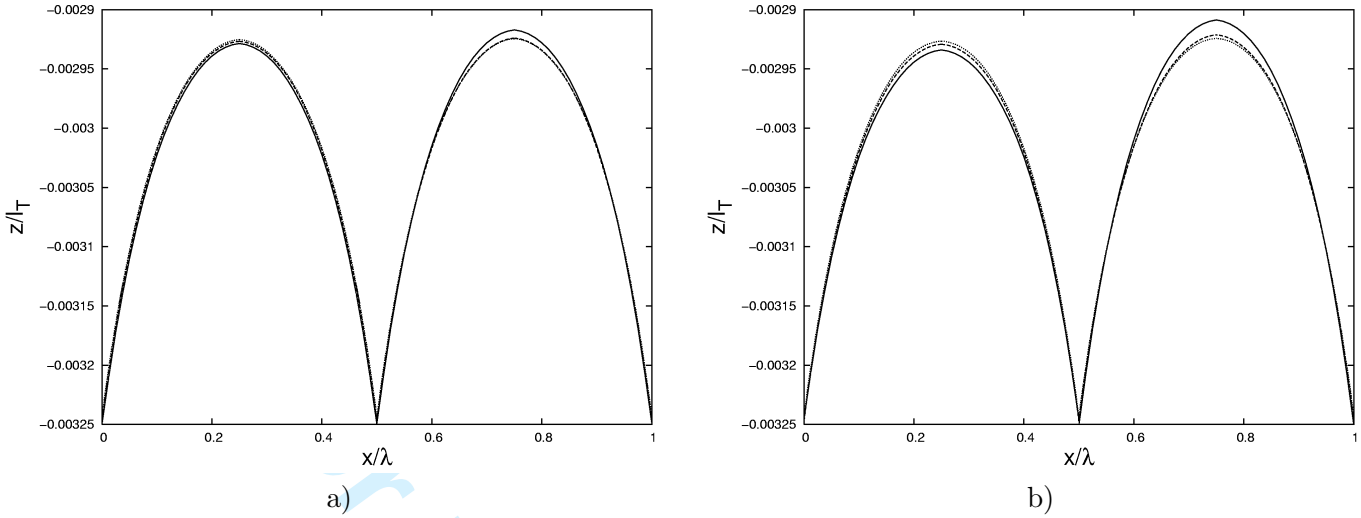

Figure 9. Steady-state lamellae growth with fluid flow. The parameters for all the runs are given in the text above. Solid line, $\lambda/W = 64$; dashed lines, $\lambda/W = 96$; dotted lines, $\lambda/W = 128$. a) $Ra = 1.34 \times 10^{-2}$ and b) $Ra = 3.85 \times 10^{-2}$.

If we examine the microstructure growth in Fig. 9 we see that they are not drastically altered by natural convection. Moreover the lamellae pair are slightly asymmetric and this asymmetry is less pronounced for small Rayleigh number (case where convections effect are smaller, see Fig. 9a)).

The asymmetry can be explained by the fact that in the presence of a gravitational field, the difference in the concentration field of α, β and liquid phase produces natural convection which induces a fluid motion in the central part of the liquid close to the interface triple point (see Fig. 10). This means that the concentration field ahead of the solid-liquid interface is not symmetric any longer. In our case, the fluid motion increases the solute transport in front of the β phase (lamellae in red, see Fig. 10) and it enriches the solute field in front of the α phase (lamellae in blue, see Fig. 10). Since these effects are quite small we can see only a slight asymmetry on the growth of the lamellae.

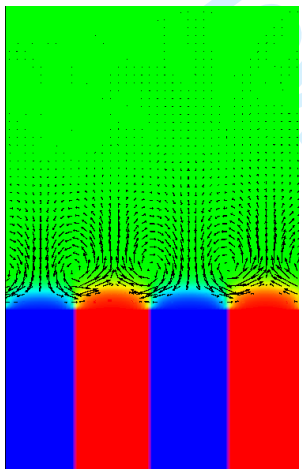

Figure 10. This picture shows a snapshot of the phase-field simulation of eutectic growth in the presence of natural convection. The arrows represent the fluid motion and the colors the concentration field. The phase α is represented by the blue color and β by red.

Now, we consider the same material and computational parameters as above and we investigate the influence of natural convection on the interfacial undercooling for varying lamellar spacing. This is done by plotting the average interfacial undercooling ΔT versus the lamellar spacing λ, which, for the purely diffusive case is known as the Jackson and Hunt curve [30]. For the resolution, we take $\lambda/W = 96$, since,

on the basis of Fig. 9 we expect results to be converged for $\lambda/W \geq 96$. The lamellar spacing λ can be changed by changing the size of the simulation box. We investigate three different pulling velocities and we use $Ra = 1.34 \times 10^{-2}$ and $Ra = 3.85 \times 10^{-2}$. In Fig. 11, 12 and 13 we plot the average undercooling versus the lamellar spacing considering the cases with and without convection effects.

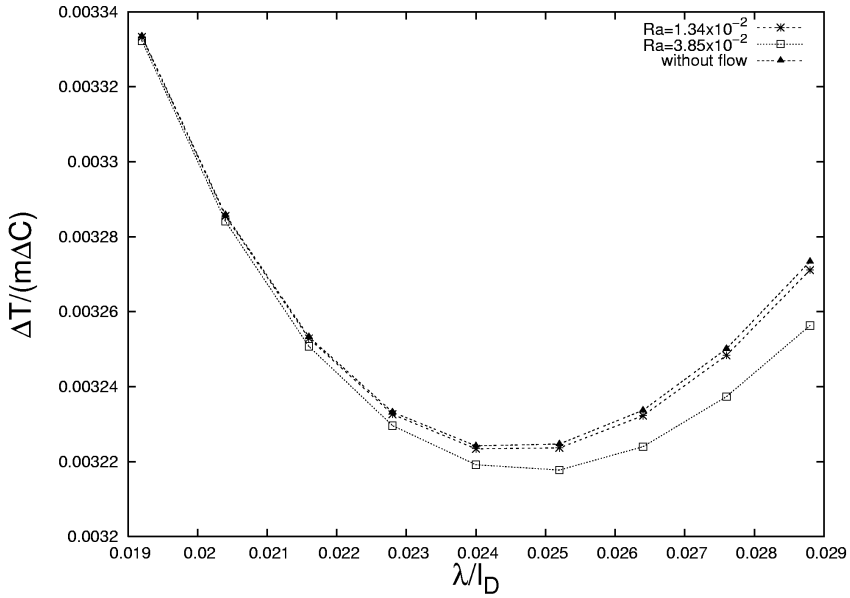

Figure 11. Average undercooling versus lamellar spacing for $l_D/\bar{d} = 45000$.

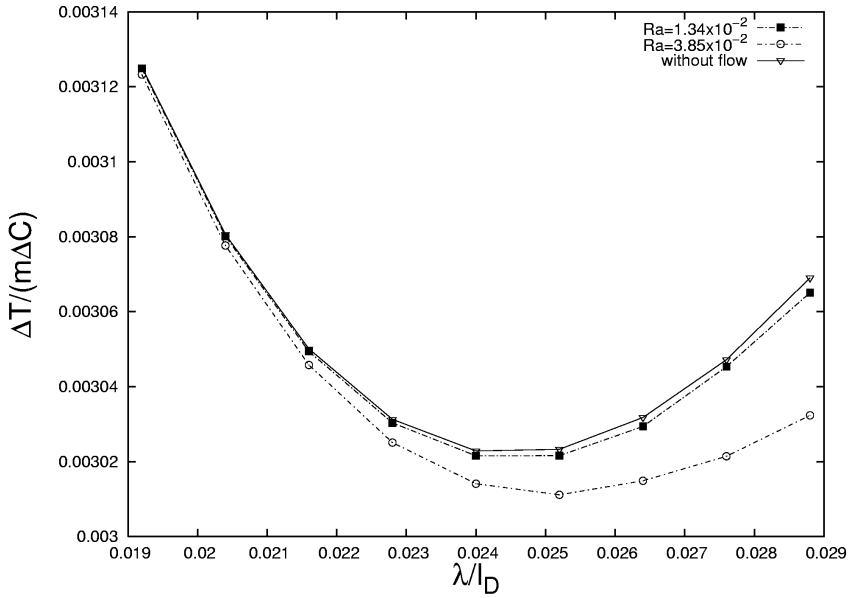

Figure 12. Average undercooling versus lamellar spacing for $l_D/\bar{d} = 51200$.

Following the Jackson and Hunt theory the interfacial undercooling has a minimum, $\Delta T = \Delta T_{JH}$, for the spacing λ_{JH}, which constitutes a reference length for lamellar eutectics. In reference [9] Folch and Plapp show a very good agreement between the Jackson and Hunt parameters (λ_{JH}/l_D and $\Delta T_{JH}/(m\Delta C)$) and the values ($\lambda/l_D$ and $\Delta T/(m\Delta C)$) computed with their phase-field model. Here we compute these values again and compare them with the minimum undercooling when convection effects are taken into account.

The results are summarized in Table 1. A graphical description of them can also be seen in Fig. 11, 12 and 13.

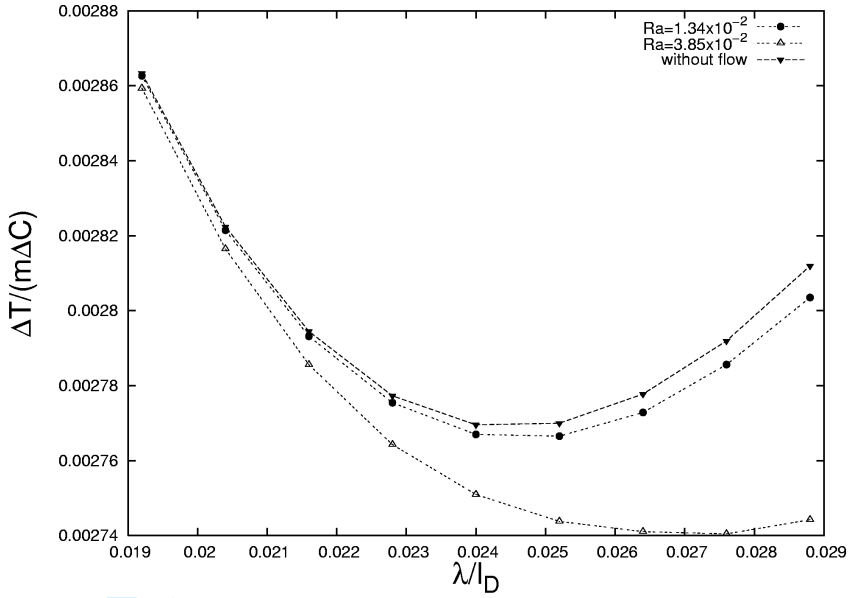

Figure 13. Average undercooling versus lamellar spacing for $l_D/\bar{d} = 61000$.

	$l_D/d = 45000$		$l_D/\bar{d} = 51200$		$l_D/\bar{d} = 61000$	
	λ_{min}	ΔT_{min}	λ_{min}	ΔT_{min}	λ_{min}	ΔT_{min}
Without flow	0.02403	0.003224	0.02403	0.003023	0.02401	0.00277
Ra_1	0.02403	0.003223	0.024402	0.003020	0.025188	0.00276
Ra_2	0.02520	0.003217	0.025201	0.003011	0.027603	0.00274

Table 1. Minimum interfacial undercooling and minimum lamellar spacing computed with the phase-field model. As a matter of simplification we represent $\lambda_{min} = (\lambda/l_D)_{min}$, $\Delta T_{min} = \Delta T/(m\Delta C)$, $Ra_1 = 1.34 \times 10^{-2}$ and $Ra_2 = 3.85 \times 10^{-2}$.

As you can take from the pictures (see Fig. 11, 12 and 13) the higher the pulling velocity the less the effect of natural forces on the minimum interfacial undercooling. In figure 11 we see almost no convection influence on the minimum interface undercooling or minimum lamellar spacing for $Ra = 1.34 \times 10^{-2}$. For $Ra = 3.85 \times 10^{-2}$ the minimum interfacial undercooling decreases and the corresponding minimum lamellar spacing increases in relation to the purely diffusive case (see also Table 1). When we decrease the pulling velocity (see Fig. 12 and 13) we still can see a stronger convection effect on the minimum interfacial undercooling and minimum lamellar spacing. As we decrease the pulling velocity, the minimum lamellar spacing in the presence of convection increases with respect to the purely diffusive case. We also observe that the effect of natural convection is more pronounced when the interfacial energy is lower.

Moreover, the results above clearly show that natural convection can modify the minimum lamellar spacing to such an extent that the Jackson and Hunt predictions are no longer valid. Similar results were also found by Zhang et al. [34] but they consider a fixed shear flow ahead of the solid-liquid interface.

4.3 *Effect of forced flow on directional solidification of eutectic lamellae*

In this section we investigate the effect of a shear flow ahead of the solid-liquid interface. Again, we use the same material parameters as in section 4.2 and resolution $\lambda/W = 96$.

In figure 14, we present numerical simulations of eutectic lamellae growth under forced convection effects. We impose a fixed shear flow $V_\infty = 7.06 \times 10^{-7} m/s$ ahead of the solid-liquid interface. The corresponding simulations for the purely diffusive case ($V_\infty = 0$) can be seen in the figure 15.

As seen from Fig. 14, forced flow rapidly alters the growth of lamellae. Whereas in the purely diffusive case (Fig. 15) the lamellae grow parallel to the z direction, in Fig. 14 we see that forced convection tilts the whole microstructure away from the flow direction. The solute field in front of the solid-liquid interface is taken away by the fluid flow, increasing the solute transport in this direction. When transverse flow

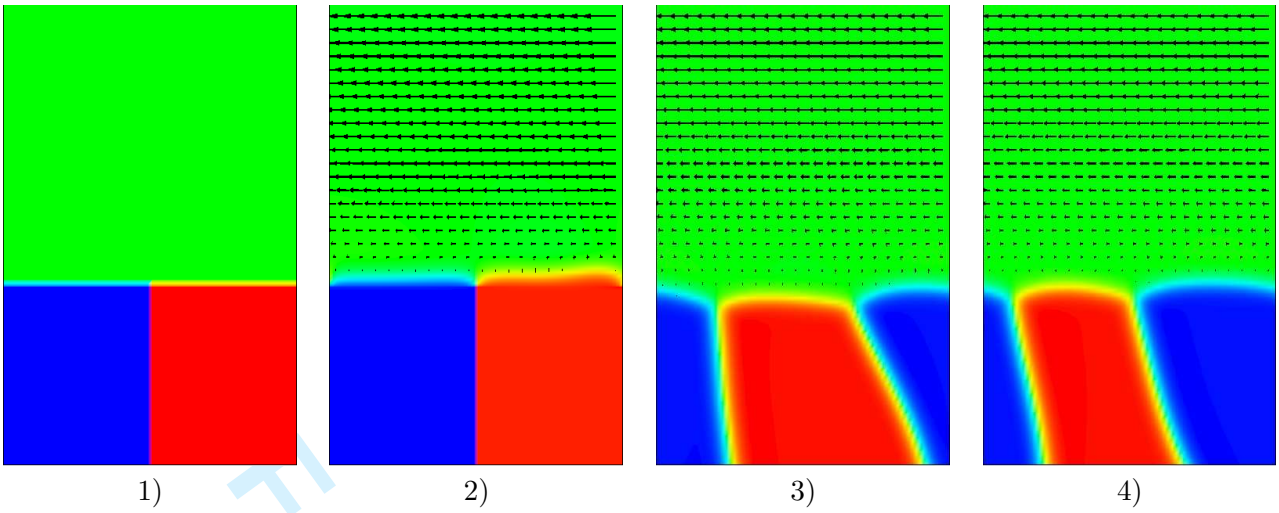

Figure 14. Time evolution of the phase-field simulations for eutectic lamellae growth with a shear flow ahead of the solid-liquid interface. Time evolves, from left to right. Note that we are showing only part of the simulation domain (the z direction is much larger than the x direction)

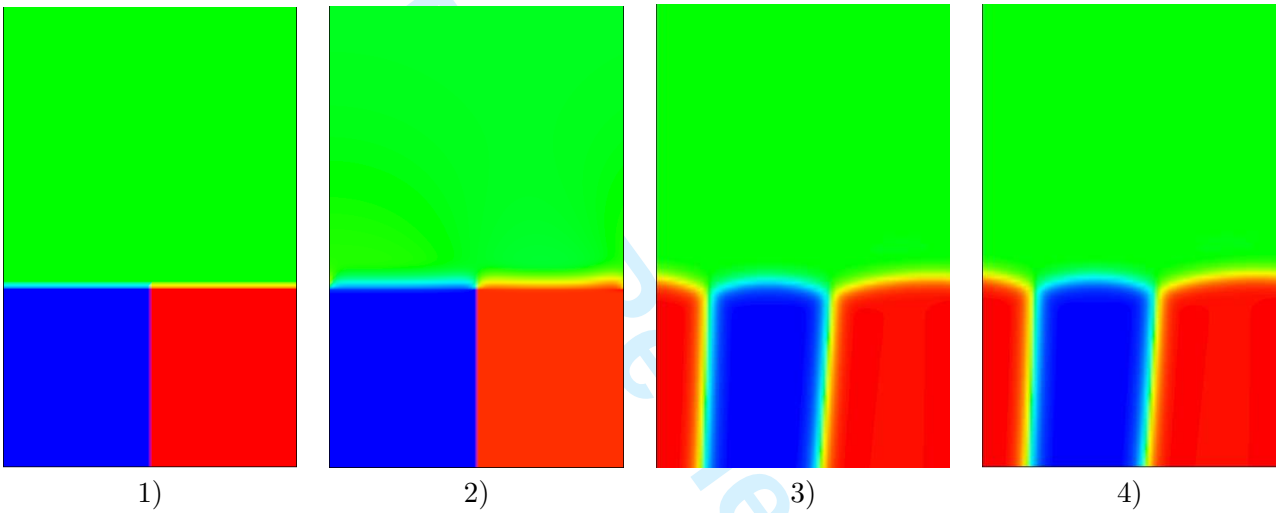

Figure 15. Time evolution of the phase-field simulations for eutectic lamellae growth under pure diffusive conditions. Time evolves, from left to right. Note that we are showing only part of the simulation domain (the z direction is much larger than the x direction)

is included in the system it increases the ability of the lateral migration of the atoms. The simulations presented in Fig. 14 correspond to the Peclet number (P_{ef}) in the range from $P_{ef} = 0.113$, based on the flow velocity near the solidifying front to $P_{ef} = 1.13$ based on the velocity ahead of the solidifying front (we choose $H = \lambda$).

More details about these investigations as well as a large range of parameter variations will be presented elsewhere in [36].

5 Peritectic growth under the influence of convection

In spite of their appearance in many metallic systems, peritectic solidification reactions and the associated microstructure development are much less understood than single phase or eutectic solidification reactions [37, 38]. Recently, considerable research efforts have been dedicated to developing alloys with intermetallic phases in search of improved material characteristics such as high strength, high ductility, and high corrosion resistance at elevated temperatures. Many of these materials are produced by peritectic solidification reactions, such as in carbon steels, Cr-Ni stainless steels, copper alloys, magnetic and

superconducting materials. The formation of a specific microstructure, determining these material characteristics, depends on a complicated interplay between initial material composition, imposed temperature gradients, growth velocity and, if present, convection in the melt [39]. Therefore it is not surprising that a wide variety of microstructures can be formed impacting materials processing and production.

Similar to an eutectic system the phase diagram of a peritectic system contains a point – the peritectic point with peritectic temperature T_p – at which two different solid phases, the parent (primary) and peritectic (secondary) phases, coexist with a liquid of higher composition than either solid phase. Above T_p, the parent phase is stable and the peritectic phase is meta-stable, whereas below T_p, the opposite is true. In the following we will consider C to be the concentration of the impurity and T_m the melting point of the pure phase. A schematic phase diagram of a peritectic material system can be seen in the figure 16.

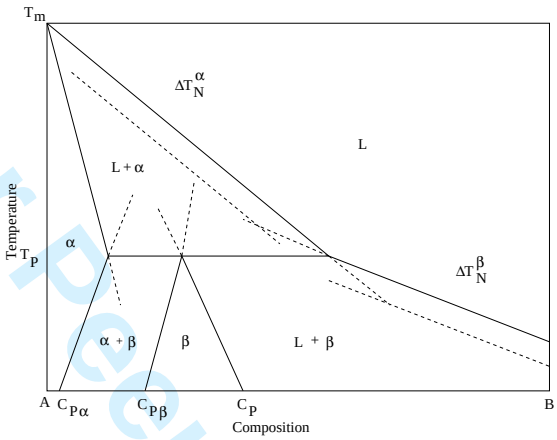

Figure 16. Schematic phase diagram of a peritectic alloy. C, concentration of impurity B; T_m, melting point of pure A; T_p, peritectic temperature. C_p, $C_{p\beta}$, and $C_{p\alpha}$ are the compositions of the liquid, β solid, and α solid that are in equilibrium at T_p. ΔT_N^α and ΔT_N^β are the nucleation undercoolings for α and β phases, respectively. Dashed lines are metastable extensions of the liquidus and solidus lines. This figure was taken from the reference [40].

Here we apply the phase-field model approach described in section 3.1 to investigate microstructure growth in a peritectic system under the influence of hydrodynamic convection in the melt.

5.1 *Numerical simulations*

The model described in section 3.1 allows us to investigate the peritectic transformation under the influence of fluid flow quantitatively. A representative evolution is shown in Fig. 17, where time runs from the left picture to the right. The row of pictures on the top represents the case where flow in the melt phase is taken into account, on the bottom the case without flow. The pictures (with and without flow) are depicted at the same time step for the same process parameters. The dark circle indicates the properitectic phase, the light structure the peritectic phase, which is nucleating on top of the properitectic one. Comparing peritectic growth with and without convection we find that hydrodynamic transport in the melt enhances the growth process considerably. To stress this effect we investigated a scale relation which describes the influence of the inflow velocity on the solid volume fraction of the microstructure evolution for a fixed time instant. In Fig. 18 we resume this finding by plotting the logarithm of the solid volume fraction versus the logarithm of the inflow velocity. We can see that for larger inflow velocity a linear regime was found. More details about these findings can be seen in [3]. Moreover, these results are in qualitative agreement with experimental investigation of the peritectic material system Fe-Ni in [41].

5.2 *Investigating natural convection on directional solidification of peritectic materials*

The phase-field model described in section 3.1 allows us to numerically simulate directional solidification of Al-36wt%Ni.

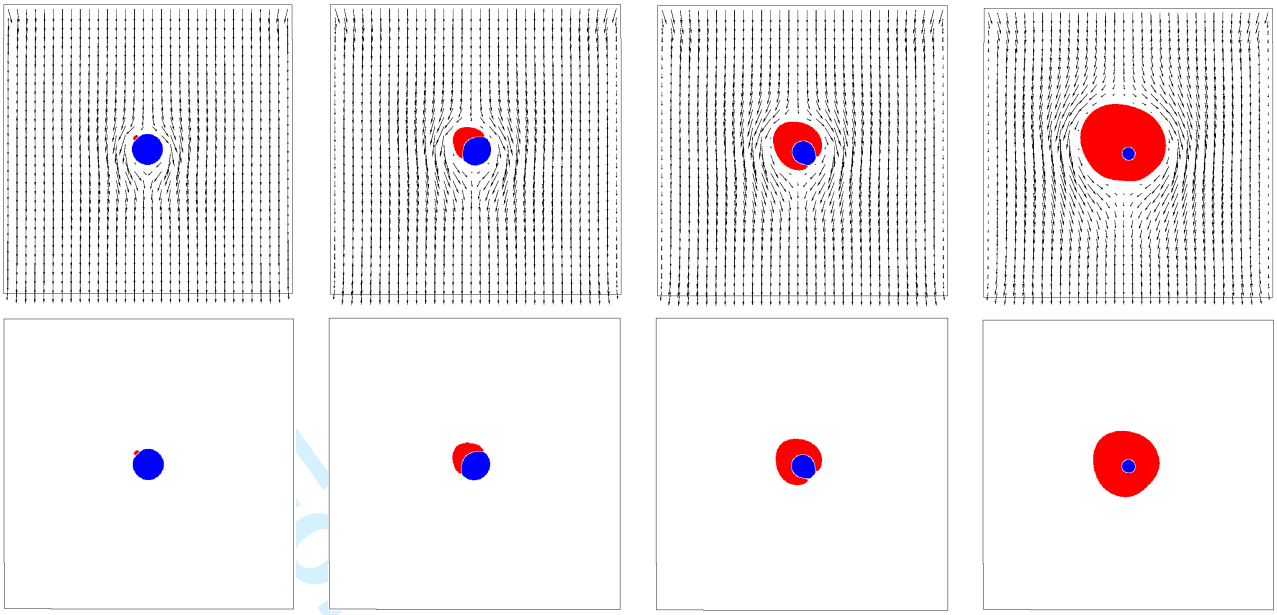

Figure 17. Numerical simulations of the peritectic transformation under the influence of convection (on the top) and without convection (on the bottom). The dark circle indicates the properitectic phase, the light structure the peritectic phase. Arrows are vectors indicating the velocity of the hydrodynamic field in the molten phase. The parameters used were: $m_\alpha = -3.73K/at\%$, $m_\beta = -0.6K/at\%$, $T_p = 1790.4K$, $D = 5.0 \times 10^{-9} m^2/s$ and the scaled concentrations $c_\alpha = -2.16$ and $c_\beta = -1.16$ [41].

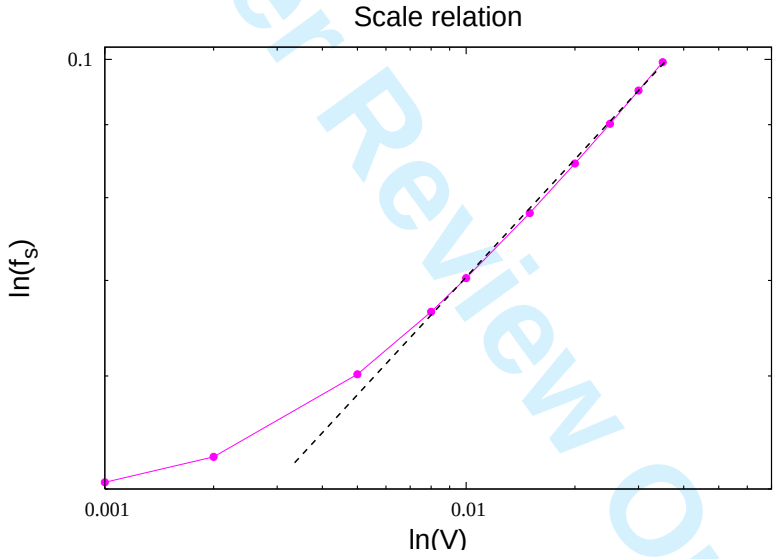

Figure 18. Plot of the logarithm of the solid volume fraction versus the logarithm of the inflow velocity.

The simulation set up starts with a piece of Al_3Ni_2 phase in a supersaturated melt (see figure 19). The width of the simulation box (perpendicular to the growth direction) is chosen equal to the experimentally determined primary dendrite arm spacing $\lambda_1 = 400\mu$m. To be able to simulate the whole dendrite structure we shifted the peritectic temperature to a value about 70K above the original one.

The phase Al_3Ni_2 is allowed to grow until a time where it is relaxed. Once the phase Al_3Ni_2 is relaxed, a piece of the Al_3Ni phase is nucleated on the interface of liquid+Al_3Ni_2 and below the peritectic temperature, T_p. Note that we follow the solidifying front by advancing the simulation box from time to time along the growth direction. Basically, we follow the growth near the peritectic temperature. The simulation window, which we use for the simulation set up, corresponds to the temperature range containing the peritectic temperature. The assumed nucleation temperature was 80 K below T_p. This causes the peritectic

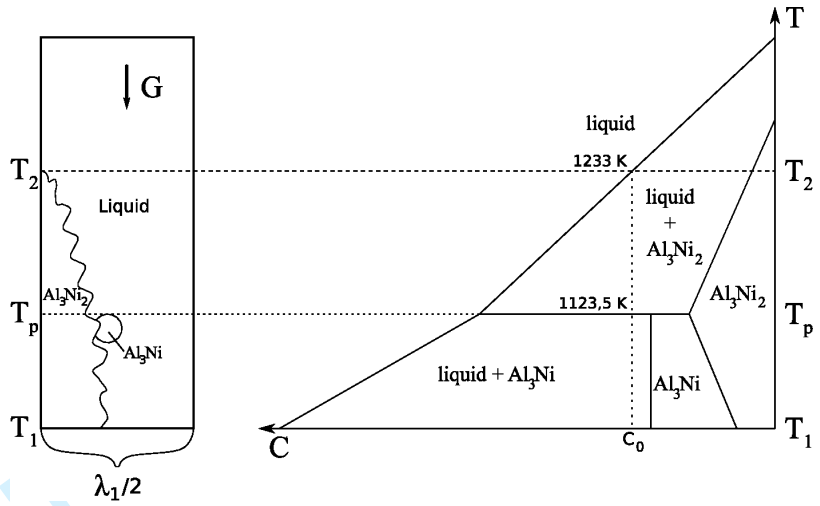

Figure 19. Schematic phase-diagram and simulation set-up.

phase to grow both along the Al_3Ni_2+Liquid interface and inside the liquid phase.

For this study we choose the diffusion constant in the liquid as $D_L = 1.0 \times 10^{-9}\text{m}^2\ \text{s}^{-1}$ and the anisotropy of the properitectic phase as $\epsilon = 0.05$. The diffusion constant in the solid phase was taken as $D_L = 1.0 \times 10^{-10}\text{m}^2\ \text{s}^{-1}$. The surface tension was assumed to be equal in both solid phases. It was taken to be $\sigma_{i,L} = 0.09\ \text{Jm}^{-2}$, which is an estimated value. We include the effect of natural convection by taking $Ra = 1.34 \times 10^{-2}$. The nucleation was described by supposing that a nucleus form at a certain critical undercooling.

In Figure 20 we simulate the time evolution of directional solidification for Al-36wt%Ni with process parameters $G = 20$ K/mm and $v_p = 100\mu\text{ms}^{-1}$. The critical temperature for nucleation of the peritectic phase was set at 4 K below the peritectic temperature. The reference temperature for the position of the dendrite tip was set in a way that the dendrite can fully develop with sidebranches. Observe that after nucleation the peritectic phase grows around the properitectic phase, but it also grows into the properitectic phase as well as into the liquid. In the last figure on the right side of figure 20 you can see that some sidebranches of the properitectic phase were almost completely consumed from the peritectic phase. In this case we do not observe any meaningful convective effect (natural convection) on the microstructure growth.

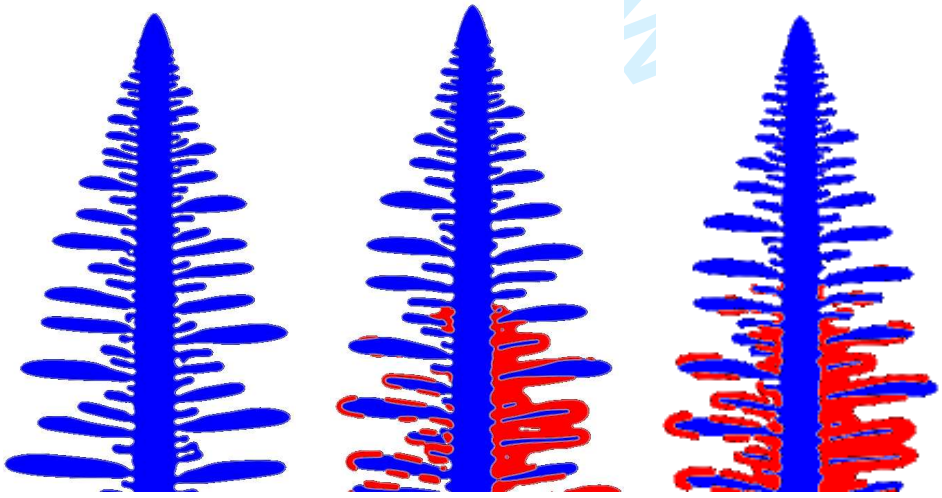

Figure 20. Growth of peritectic intermetallic phase from the dendritic Al_3Ni inside the mushy-zone. Time evolves from left to right. We use G=100 K/mm and . Dark grey represents the dendritic phase Al_3Ni_2 and mid grey the Al_3Ni phase. The solutal Rayleigh number was taken as $Ra = 1.34 \times 10^{-2}$.

6 Discussion

In this work we have extended a quantitative phase-field approach [10] to simulate dendritic growth of a Fe-9.8mol%Mn alloy under the influence of an imposed flow field. We have shown the influence of (macroscopic) convection on the pattern formation on the scale of the microstructure. On the one hand, convection alters the morphology of dendrites, by influencing, for instance, the solute boundary layer thickness and the solute pile-up. On the other hand, in the neighborhood of a dendrite, convection can result in the enrichment/impoverishment of solute in the liquid phase. This alters the (local) supersaturation on the microscale, and this influences some characteristics of dendritic growth, e.g. tip velocity, sidebranching, but also the local evolution of the solid fraction. We have presented phase-field simulations of eutectic lamellae growth under the effect of natural convection and the effect of a transverse shear flow fixed ahead of the solid-liquid interface. Moreover, we have done convergence studies by analyzing the lamellar steady state growth including convection in the molten phase. We show that even when taking the non-linear effects due to fluid flow in the melt into account, the phase-field model still exhibits thin-interface corrections. We have also demonstred that natural convection can change the minimum lamellar spacing and that this will depend on the process parameters. In the case of transverse flow we have shown that fluid flow tilts the eutectic lamellae away from the flow direction, changing the whole microstructure in comparison to the case without fluid flow effects. The likewise important message here is that we have build a quantitative phase-field model which is able to simulate numerically eutectic growth under the effect of convection. Furthermore, we applied our phase-field approach successfully to investigate the influence of melt flow on the peritectic transformation.

References

[1] A. Karma, W. -J. Rappel, Phys. Rev. E, 57 4323 1998.
[2] P. Zhao, J.C. Heinrich and D. R. Poirier, Int. J. Numer. Meth. Fluids, 49 233 2005.
[3] R. Siquieri and H. Emmerich, Phil. Magazine Lett. 87, 11 829 2007.
[4] H. Emmerich, Advances in Physics, 57 1 2008.
[5] H. Emmerich, *The Diffuse Interface Approach in Material Science - Thermodynamic Concepts and Applications of Phase-Field Models, Lecture Notes in Physics*, Springer-Verlag, Berlin, LNPm 73 2003.
[6] A. Karma and W. -J. Rappel, Phys. Rev. E, 53 3017 1996.
[7] W. Kurz and D. J. Fischer, *Fundamentals of solidification,* Trans Tech Publications, Aedermansdorf, 1986.
[8] R.F. Almgren, SIAM J. Appl. Math. 59:2086, 1999.
[9] R. Folch and M. Plapp, Phys. Rev. E, 72 011602 2005.
[10] B. Echebarria, R. Folch, A. Karma and M. Plapp, Phys. Rev. E, 70 061604 2004.
[11] A. Karma, Phys. Rev. Lett., 87 115701 2001.
[12] D. Medvedev and K. Kassner, J. Cryst. Growth, 275 1496 2005.
[13] N. Zabaras, B. Ganapathysubramanian and L. Tan, J. Comp. Phys., 218 200 2006.
[14] S. R. Coriell, G. B. McFadden, W.F. Mitchell, B. T. Murray, J. B. Andrews and Y. Arikawa, J. Cryst. Growth, 224 145 2001.
[15] R. Tönhardt and G. Amber, J. Cryst. Growth, 194 406 1998.
[16] D. Medvedev and K. Kassner, Phys. Rev. E, 72 056703 2005.
[17] D. Medvedev, T. Fischaleck and K. Kassner, Phys. Rev. E, 74 031606 2006.
[18] X. Tong, C. Beckermann, A. Karma and Q. Li, Phys. Rev. E, 63 061601 2001.
[19] C. Beckermann, H. -J. Diepers, I. Steinbach et. al, J. Comp. Phys., 154 468 1999.
[20] R. Siquieri, H. Emmerich and M. Jurgk, Eur. Phys. J. Special Topics, 149 27 2007.
[21] E. Bänsch and A. Schmidt, Inter. and Free Boundaries, 2 95 2000.
[22] M. Griebel, T. Dornseifer and T. Neunhoeffer, *Numerical simulation in fluid dynamics*, SIAM, Philadelphia, 1997.
[23] A. A. Amsden and F. H. Harlow, J. Comp. Phys., 6 332 1970.
[24] K. Atkinson, *An introduction to numerical analysis*, John Wiley, 2nd, 1989.
[25] P. -R. Cha, D. -H. Yeon and J. -K. Yoon, Acta Mate., 49 3295 2001.
[26] Vinnikov, L.Yu. Georgieva and L.G. Maisterenko, Metallofizika 55:24, 1974.
[27] H. Emmerich and R. Siquieri, J. Phys.-Cond. Matt. 18, 49 1112 2006.
[28] L. L. Regel and W. R. Wilcox, D. Popov and F. Li, Acta Astronautica, 48 101 2001.
[29] J. H. Lee, S. Liu and R. Trivedi, Metall. and Mater. Trans. A, 36A 3111 2005.
[30] K. A. Jackson and J. D. Hunt, Trans. AIME, 236 1129 1966.
[31] D. Ma, W. Q. Jie, Y. Li and S. C. NG, Acta Mater., 46 3203 1998.
[32] D. J. Larson, In ASTP Summary Science Report NASA, 449 1976.
[33] V. Baskaran and W. R. Wilcox, J. Cryst. Growth, 67 343 1984.
[34] W. Zhang, H. Fu, Y. Yang and Z. Hu, J. Cryst. Growth, 194 263 1998.
[35] M. Ginibre, S. Akamatsu and G. Faivre, Phys. Rev. E, 56 780 1997.
[36] R. Siquieri and H. Emmerich, in preparation.
[37] Kerr, H. W., International Material Reviews 41 129 1996.
[38] T. Umeda, T. Okane and W. Kurz, Acta Mater., 44 4209 1996.
[39] T. a. Lograsso, B. C. Fuh and R. Trivedi, Metall. Mater. Trans.A. 36 1287 2005.
[40] T. S. Lo, A. Karma and M. Plapp, Phys. Rev. E, 63 031504 2001.

[41] M. Vandyoussefi, H. W. Kerr and W. Kurz, Acta Mater., 48 2297 2000.